Controlling magnetic exchange and anisotropy by nonmagnetic ligand substitution in layered MPX_3 (M = Ni, Mn; X = S, Se)

Rabindra Basnet,[1] Kamila M. Kotur,[3] Milosz Rybak,[4] Cory Stephenson,[1] Samuel Bishop,[5,*] Carmine Autieri,[6,7,†] Magdalena Birowska,[3,‡] and Jin Hu[1,2,§]

[1]*Department of Physics, University of Arkansas, Fayetteville, Arkansas 72701, USA*
[2]*Institute for Nanoscience and Engineering, University of Arkansas, Fayetteville, Arkansas 72701, USA*
[3]*Faculty of Physics, University of Warsaw, Pasteura 5, PL-02093 Warsaw, Poland*
[4]*Department of Semiconductor Materials Engineering, Faculty of Fundamental Problems of Technology, Wroclaw University of Science and Technology, Wybrzeże Wyspiańskiego 27, PL-50370 Wroclaw, Poland*
[5]*Haas Hall Academy, Fayetteville, Arkansas 72701, USA*
[6]*International Research Centre Magtop, Institute of Physics, Polish Academy of Sciences, Aleja Lotników 32/46, PL-02668 Warsaw, Poland*
[7]*Consiglio Nazionale delle Ricerche CNR-SPIN, UOS Salerno, I-84084 Fisciano (SA), Italy*

(Received 24 April 2022; accepted 27 May 2022; published 29 June 2022)

Recent discoveries in two-dimensional magnetism have intensified the investigation of van der Waals magnetic materials and further improved our ability to tune their magnetic properties. Tunable magnetism has been widely studied in antiferromagnetic metal thiophosphates MPX_3. Substitution of metal ions M has been adopted as an important technique to engineer the magnetism in MPX_3. In this work, we have studied the previously unexplored chalcogen X substitutions in MPX_3 (M = Mn/Ni; X = S/Se). We synthesized the single crystals of $MnPS_{3-x}Se_x$ ($0 \leqslant x \leqslant 3$) and $NiPS_{3-x}Se_x$ ($0 \leqslant x \leqslant 1.3$) and investigated the systematic evolution of the magnetism with varying x. Our study reveals the effective tuning of magnetic interactions and anisotropies in both $MnPS_3$ and $NiPS_3$ upon Se substitution. Such efficient engineering of the magnetism provides a suitable platform to understand the low-dimensional magnetism and develop future magnetic devices.

DOI: 10.1103/PhysRevResearch.4.023256

I. INTRODUCTION

The recently discovered two-dimensional (2D) magnetic materials have attracted intensive attention because of the possible new phenomena arising from 2D magnetism and the promising potential for spintronic applications [1–6]. The integration of 2D magnets in nanodevices and heterostructures has further fueled the investigation of their magnetic and electronic properties, thus offering a fertile platform to design next-generation devices [7–19]. Such developments in 2D magnetism have motivated the search for novel magnetic van der Waals (vdW) materials to explore the low-dimensional magnetism in real materials.

One interesting class of magnetic vdW materials is antiferromagnetic (AFM) MPX_3 (M = transition metal ions, X = chalcogen ions), in which the transition metal ions carry localized magnetic moments in a layered honeycomb lattice [20–23]. Their magnetic properties are strongly influenced by the transition metal M. The magnetic exchange and anisotropy are found to vary with the choice of M [23–40]. Such tuning of magnetism by altering M has led to the study of a series of polymetallic "mixed" MPX_3 compounds such as $Ni_{1-x}Mn_xPS_3$, $Mn_xFe_{1-x}PS_3$, $Fe_{1-x}Ni_xPS_3$, $Mn_{1-x}Zn_xPS_3$, $Ni_{1-x}Co_xPS_3$ and $Mn_{1-x}Fe_xPSe_3$ [34,37,39,41–53]. Tunable magnetism arising from the interplay between competing magnetic interactions, magnetic anisotropy, and spin fluctuations has been observed in these mixed compounds [34,37,39,41–52], providing promising candidates to explore novel phenomena originating from 2D magnetism.

Compared with the metal substitution in the M site [34,37,39,41–53], chalcogen substitution in the X site leaves the magnetic ions intact, hence offering a relatively clean approach to modify the magnetic exchange interactions. The effectiveness of substituting nonmagnetic ligand atoms to engineer the magnetism in vdW magnets has been demonstrated recently [54,55]. For example, in chromium halide, varying the ratio of halides is found to effectively control the ordering temperature and magnetic anisotropy [54]. Furthermore, the competing spin-orbit coupling strength of Cr and halides leads to a new frustrated regime and modified interlayer coupling in $CrCl_{3-x-y}Br_xI_y$ [55]. However, the chalcogen-substitution effects on magnetism remain elusive in MPX_3, with only a few syntheses and structural characterization works have been reported [56–59].

*Present address: Williams College, Massachusetts 01267, USA.
†autieri@magtop.ifpan.edu.pl
‡birowska@fuw.edu.pl
§jinhu@uark.edu

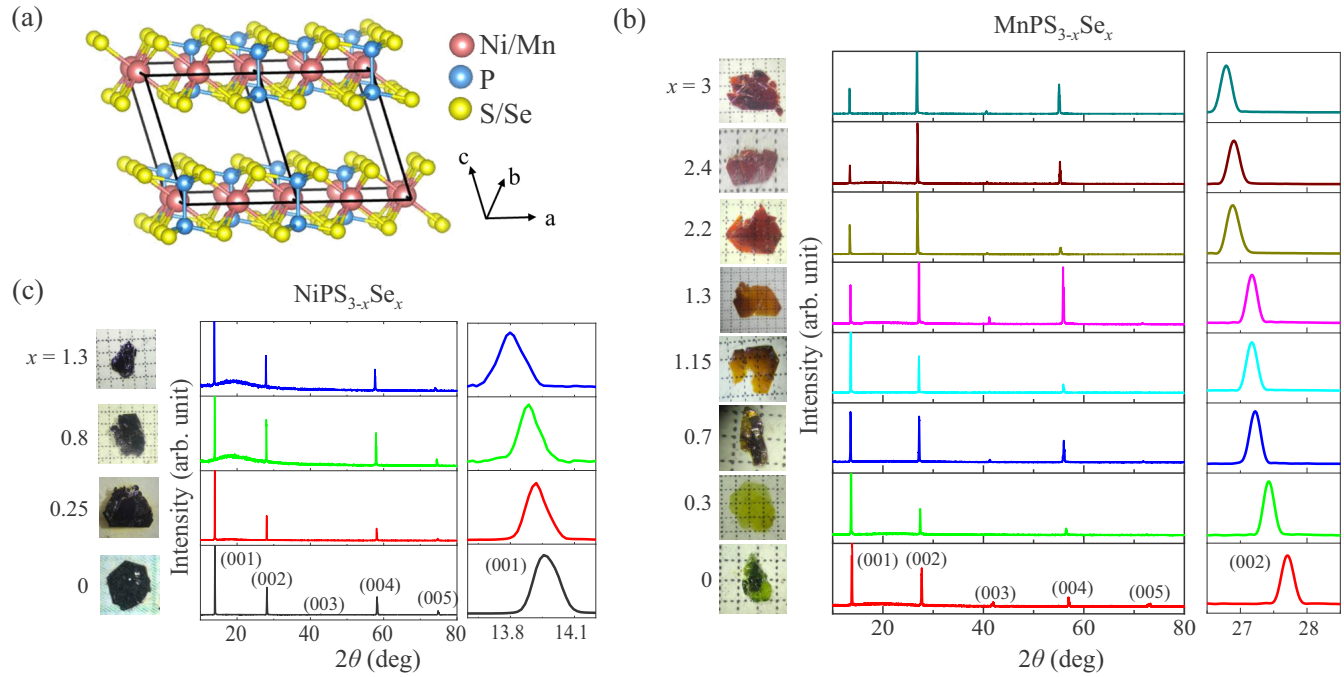

FIG. 1. (a) Crystal structure of MPX_3 (M = Mn/Ni; X = S/Se). (b) Optical microscope images of the as-grown single crystals and Single-crystal x-ray-diffraction pattern of $MnPS_{3-x}Se_x$ ($0 \leqslant x \leqslant 3$) showing the (00$L$) reflections. Right panels show (002) diffraction peak. (c) Optical microscope images of the as-grown single crystals and single-crystal x-ray-diffraction pattern of $NiPS_{3-x}Se_x$ ($0 \leqslant x \leqslant 1.3$) showing the (00$L$) reflections. Right panels show (001) diffraction peak. The value of Se content x for each sample is determined by EDS.

In this work, we conducted a systematic study on the magnetic properties of $MnPS_{3-x}Se_x$ and $NiPS_{3-x}Se_x$ ($0 \leqslant x \leqslant 3$). We found very different doping dependences for Néel temperature (T_N) in those two material systems, likely due to the difference in their dominant exchange interactions i.e., direct M-M interaction in $MnPS_3$ whereas superexchange M-X-M interaction in $NiPS_3$. Furthermore, chalcogen substitution also effectively controls the magnetic anisotropy, which is manifested by the efficient tuning of the magnetic easy axis and spin flop (SF) transition. Such tunable magnetism achieved by nonmagnetic substitutions offers a useful technique to engineer low-dimensional magnetism and provides further insights for the development of magnetic materials-based nanodevices.

II. EXPERIMENT

The $MnPS_{3-x}Se_x$ and $NiPS_{3-x}Se_x$ single crystals used in this work were synthesized by a chemical vapor transport method using I_2 as the transport agent. Elemental powders with desired ratios were sealed in a quartz tube and heated in a two-zone furnace for a week. The $MnPS_{3-x}Se_x$ single crystals were grown with a temperature gradient from 650 to 600 °C, whereas 750 to 550 °C was used for $NiPS_{3-x}Se_x$ growth. The polycrystalline $NiPS_{3-x}Se_x$ samples used in this work were grown using a self-flux method at 750 °C. The as-grown polycrystalline samples were annealed at 750 °C for 4 days to minimize the possible impurity phase. Such annealing process is necessary to obtain a pure phase for characterizing magnetic properties. The elemental compositions and crystal structures of the obtained crystals were examined by energy-dispersive x-ray spectroscopy (EDS) and x-ray diffraction (XRD), respectively. Magnetization measurements were performed in a physical property measurement system (PPMS, Quantum Design).

The calculations were performed in the framework of the density functional theory (DFT)+U [60] approach as implemented in VASP software [61,62]. The effective on-site Coulomb exchange parameters were set to $U = 5$ eV and $U = 6$ eV for $3d$ states of Mn and Ni atoms, respectively. A cutoff of 400 eV was chosen for the plane-wave basis set and a **k** mesh of $10\times6\times2$ and $10\times6\times9$ was taken to sample the first Brillouin zone on Γ-centered symmetry reduced Monkhorst-Pack mesh for monolayer and bulk systems, respectively. The denser **k**-mesh grids equal to $15\times9\times13$ was taken with spin-orbit coupling (SOC) included. The standard exchange-correlation functionals neglect the nonlocal nature of dispersive forces, which are crucial for layered materials and adsorption molecules on the surfaces [63–65]. Thus, the semiempirical Grimme method was applied [66]. The lattice parameters have been fixed to the experimental ones. The positions of the atoms were relaxed until the maximal force per atom was less than 10^{-3} eV/Å. The noncollinear magnetism and SOC were included in our calculations.

III. RESULTS AND DISCUSSION

In each layer of MPX_3, the transition metals M are surrounded by P_2X_6 clusters as shown in Fig. 1(a). So, the chalcogen substitution in the X site would modify the local environment of M^{2+} within honeycomb layers. Our extensive crystal growth efforts have resulted in sizable single crystals of $MnPS_{3-x}Se_x$ with x up to 3 (i.e., full replacement of S by Se). As shown in Fig. 1(b), these crystals are relatively

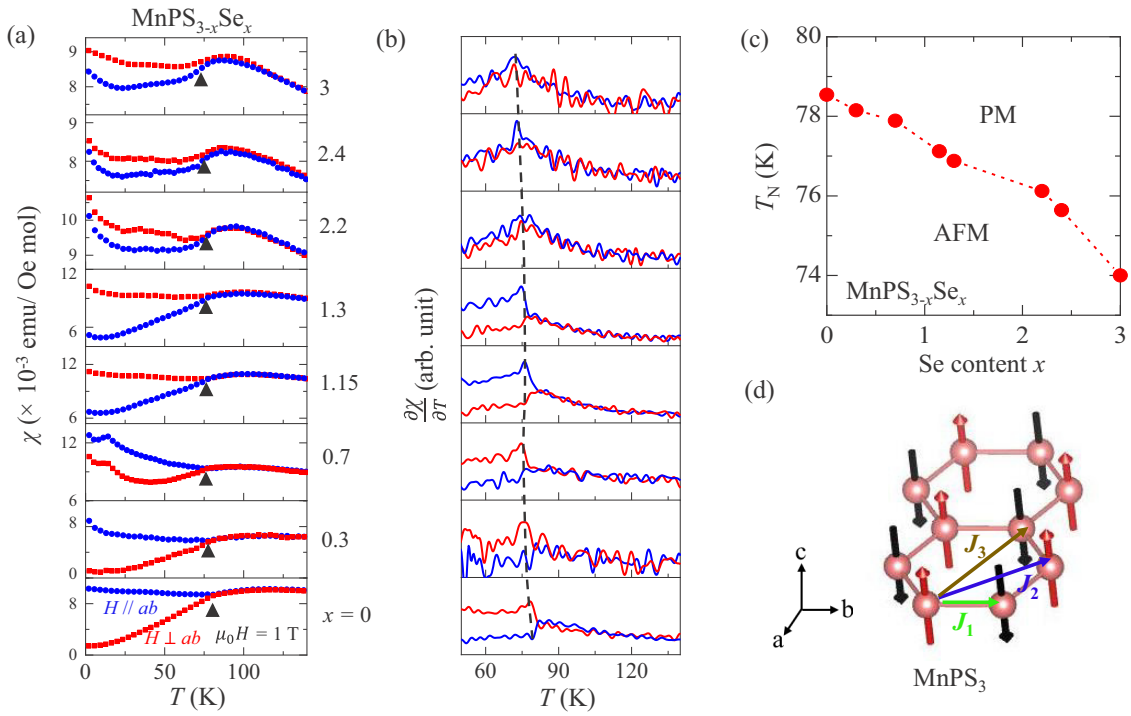

FIG. 2. (a) Temperature dependence of out-of-plane ($H\perp ab$, red) and in-plane ($H\|ab$, blue) molar susceptibility (χ) of $MnPS_{3-x}Se_x$ ($0 \leqslant x \leqslant 3$) samples. The black triangles denote T_N. (b) Temperature dependence of derivative $d\chi/dT$ of $MnPS_{3-x}Se_x$ samples. The dashed lines denote T_N. (c) Doping dependence of Néel temperature (T_N) for $MnPS_{3-x}Se_x$. (d) Magnetic structure of pristine $MnPS_3$ showing nearest-neighbor (J_1), second nearest-neighbor (J_2), and third nearest-neighbor (J_3) interactions.

transparent, showing a gradual color change from green ($x=0$) to wine red ($x=3$), which indicates the variation of the optical gap. On the other hand, for $NiPS_{3-x}Se_x$, good single crystals can only be obtained for x up to 1.3 [Fig. 1(c)]. Such difficulty in growing single crystals for Se-rich samples could be the reason for the very limited studies on $NiPSe_3$ [67] as compared to $NiPS_3$. The successful substitution in both $MnPS_{3-x}Se_x$ and $NiPS_{3-x}Se_x$ is demonstrated by the composition analyses using EDS. Furthermore, As shown in Figs. 1(b) and 1(c), the (00L) XRD peaks show systematic low-angle shift with increasing the Se content, consistent with the elongation of c axis when smaller S is replaced by larger Se.

To investigate the effects of Se substitution on magnetic properties, we measured the temperature dependence of molar susceptibility (χ) for $MnPS_{3-x}Se_x$ and $NiPS_{3-x}Se_x$ under the out of plane ($H\perp ab$) (red color) and in-plane ($H//ab$) (blue color) magnetic fields [Figs. 2(a) and 3(a)]. To obtain the precise transition temperature for each sample, we used the peak position of the derivative $d\chi/dT$ to define T_N [Figs. 2(b) and 3(b)], which has also been widely used in previous studies [39,51,53,68]. As shown in Figs. 2(a) and 3(a), the out-of-plane ($\chi_\perp$) and in-plane ($\chi_{//}$) susceptibility for both $MnPS_{3-x}Se_x$ and $NiPS_{3-x}Se_x$ overlap in the paramagnetic (PM) state but start to deviate below T_N (denoted by black triangles). In earlier studies, both substantial [24,39,53,69] and the lack [25,33,35,51,68] of magnetic anisotropy in the PM state have been reported. It has also been pointed out that the sample holder may contribute to the observed magnetic anisotropy, especially for the $NiPS_3$ samples whose magnetization is relatively weak [25]. Therefore, we have been very careful in the magnetization measurements, for which we used the same quartz sample holder for both $\chi_\perp$ and $\chi_{//}$ measurements. For Se-rich $NiPS_{3-x}Se_x$ ($x = 2$ and 3) [Fig. 3(a)], T_N is obtained from the measurements on polycrystalline samples so that $\chi_\perp$ and $\chi_{//}$ cannot be obtained. The extracted T_N for the end compounds ($x = 0$ or 3) $MnPS_3$, $MnPSe_3$, $NiPS_3$, and $NiPSe_3$ are 78.5, 74, 155, and 212 K, respectively, consistent with the previous studies [23,25,27,29,32,50,67,70,71].

Substituting S by Se leads to systematic variations of T_N in both material systems. Such T_N evolution is completely different from that caused by metal substitutions in $MnPS_3$ and $NiPS_3$ [34,37,39,46]. In polymetallic mixed compounds such as $Ni_{1-x}Mn_xPS_3$ [37,39], $Mn_xFe_{1-x}PS_3$ [46], and $Mn_{1-x}Zn_xPS_3$ [34], T_N is drastically reduced by substituting magnetic or nonmagnetic metal ions, reaching minimum around $x = 0.5$. However, chalcogen substitution only slightly reduces T_N in $MnPS_{3-x}Se_x$, from 78.5 K for $MnPS_3$ to 74 K for $MnPSe_3$ [Figs. 2(a) and 2(c)]. For $NiPS_{3-x}Se_x$, Se substitution causes T_N to increase monotonically [Figs. 3(a) and 3(c)], which is distinct from the sharp decrease in metal substituted $NiPS_3$ [37,39]. As will be discussed below, the observed evolutions of T_N with chalcogen substitutions in these two material systems can be understood in terms of the anion-mediated superexchange interactions in addition to the direct M-M exchange. The distinct doping dependences of T_N in those compounds can be attributed to their different magnetic interactions [72,73].

In MPX_3 compounds, substituting S by larger Se expands the in-plane lattice [59,74] and leads to the attenuation of the direct M-M interaction within the metal ion plane [59,65]. In $MnPS_3$, the neighboring Mn moments are found to be

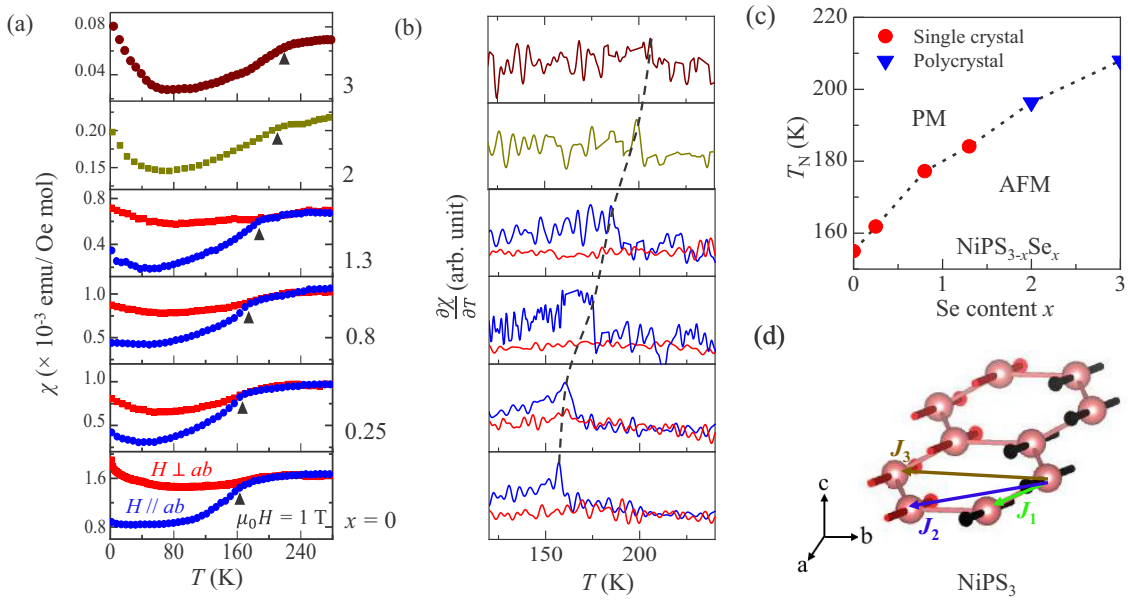

FIG. 3. (a) Temperature dependence of out-of-plane ($H \perp ab$, red) and in-plane ($H \| ab$, blue) molar susceptibility (χ) of $NiPS_{3-x}Se_x$ ($0 \leqslant x \leqslant 3$) samples. The dark yellow and wine color data represent $x = 2$ and 3 polycrystals samples, respectively. The black triangles denote T_N. (b) Temperature dependence of derivative $d\chi/dT$ of $NiPS_{3-x}Se_x$ samples. The dashed lines denote T_N. (c) Doping dependence of Néel temperature (T_N) of $NiPS_{3-x}Se_x$. (d) Magnetic structure of pristine $NiPS_3$ showing nearest-neighbor (J_1), second nearest-neighbor (J_2), and third nearest-neighbor (J_3) interactions.

antiparallel and normal to the basal plane [36,43,75] with an AFM propagation vector $\mathbf{k} = [000]$ [75], as illustrated in Fig. 2(d). The magnetism in this compound is known to be governed by the Mn-Mn direct exchange interaction [67,72,73]. Therefore, the systematic suppression of T_N by Se substitution in $MnPS_{3-x}Se_x$ can be attributed to the weakened direct exchange interaction between the nearest-neighbor Mn ions, due to the elongated Mn-Mn bond. Indeed, weaker Mn-Mn exchange in $MnPSe_3$ in comparison to $MnPS_3$ has been theoretically proposed [67] and experimentally demonstrated by neutron scattering experiment [70].

To clarify the evolution of magnetic exchange interactions (J) upon chalcogen substitutions, we performed the DFT calculations. In order to evaluate the Néel temperatures of bulk $MnPS_3$, $MnPSe_3$, $NiPS_3$ and $NiPSe_3$ structures, we first examine the various magnetic ordering such as antiferromagnetic ones: Néel (AFM-N), zigzag (AFM-z), stripy (AFM-s), and ferromagnetic (FM) one, as reported in another work [76]. We consider the in-plane and out-of-plane directions of the spins, following the previous report [77]. Namely, we consider the Heisenberg Hamiltonian with a single ion anisotropy A:

$$H = E_0 - \frac{1}{2}\sum_{ij} J_{ij}\bar{S}_i\bar{S}_j - \frac{1}{2}\sum_{ij}\lambda_{ij}S_i^z S_j^z - A\sum_i (S|i^z)^2, \tag{1}$$

where ½ accounts for the double-counting, E_0 denotes the energy of the nonmagnetic system, S_i is a spin magnetic moment of the atomic site i. J_{ij} and λ_{ij} are the isotropic and anisotropic exchange couplings between the atomic site i and j, respectively. The off-diagonal isotropic exchange terms have been neglected. The details of these calculations along with derived equations are presented in Appendix. Here, we consider the magnetic exchanges in the monolayer systems up to the third nearest neighbors, neglecting the exchange coupling from adjacent layers. Finally, the Néel temperature has been evaluated in the mean-field approach [72], which takes the following form:

$$T_N^{Mn} = S(S+1)(-3J_1 - 6J_2 - 3J_3)/(3k_B), \tag{2}$$

$$T_N^{Ni} = S(S+1)(J_1 - 2J_2 - 3J_3)/(3k_B) \tag{3}$$

for the Mn and Ni compounds, respectively. The difference between Eqs. (2) and (3) is attributed to the different magnetic order of these two compounds. Note that the different sign of J_1 in Eqs. (2) and (3) produces a different dependence of the T_N from J_1. Where spin S is equal to 5/2 and 1 for Mn and Ni, respectively, and k_B is the Boltzmann constant. Similar expressions have been obtained in an earlier work [72]. The results are collected in Table I and are in excellent agreement with previous studies [72,73,78]. Note that the Néel temperatures obtained here are overestimated, which is a well-known fact for the systems which exhibit strong critical fluctuations. Although these critical values are overestimated as expected from the mean-field approximation, the change between the Se and S systems reflects qualitatively the change of the critical temperatures whenever the S atoms are substituted by Se. As shown in Table I, the calculated nearest-neighbor interaction (J_1) and third nearest-neighbor interaction (J_3) are reduced upon replacing Se for S in $MnPX_3$, suggesting the suppression of in-plane exchange interaction on Se substitution, which is in line with the neutron scattering experiment [70]. Note, that for both $MnPSe_3$ and $NiPSe_3$ the bond angle between the M-Se-M atoms is closer to 90° in

TABLE I. The exchange couplings J_i, the strength of a single ion anisotropy A and M-X-M bond angle using DFT calculations assuming the experimental lattice parameters. Positive (negative) values of J_i and A indicate the FM (AFM) couplings and out-of-plane (in-plane) direction of spins, respectively. The critical temperature is evaluated in the mean-field approach. For the explanation of the bond angle M-X-M see the Fig. 7.

Structure	J_1 (meV)	J_2 (meV)	J_3 (meV)	λ_1 (meV)	λ_2 (meV)	λ_3 (meV)	A (meV)	T_N (K)	$\sphericalangle M$-X-M (°)
$MnPS_3$ ($a = 6.07$ Å, $b = 10.55$ Å)	−1.22	−0.06	−0.43	-4×10^{-5}	-4×10^{-5}	7×10^{-5}	−0.005	181	83.29
$MnPSe_3$ ($a = b = 6.32$ Å)	−1.07	−0.06	−0.24	-3×10^{-3}	-4×10^{-3}	-2×10^{-3}	−0.037	145	83.34
$NiPS_3$ ($a = 5.81$ Å, $b = 10.07$ Å)	3.53	0.33	−14.06	8×10^{-4}	-8×10^{-4}	2×10^{-3}	−0.108	349	85.13
$NiPSe_3$ ($a = 6.15$ Å, $b = 10.66$ Å)	4.53	−0.13	−16.11	-5×10^{-3}	-3×10^{-2}	9×10^{-3}	0.271	411	86.40

comparison to their corresponding Sulphur structures, see Table I, pointing to the enhancement of the nearest neighbor FM superexchange according to Goodenough-Kanamori-Anderson rules [79,80]. Here, we did not comment on the changes in the second nearest-neighbor interaction (J_2) because it is negligible in both Mn and Ni systems as reported in Table I. Such attenuation of in-plane magnetic interactions can explain the experimental observation of declining T_N with Se substitution in $MnPS_{3-x}Se_x$.

The situation is different in Se-substituted $NiPS_3$. Earlier neutron scattering experiments [67,72] have demonstrated that the magnetic interactions in $NiPS_3$ occur only through a superexchange pathway. The direct exchange among the metal ions, however, does not exist because of the filled t_{2g} orbitals for Ni^{2+} [67,72]. Therefore, though direct exchange usually significantly influences J_1 in magnetic materials, J_1 in $NiPS_3$ is superexchange in nature [72,73,78] and weakly dependent on the Ni-Ni distance [81]. The observed systematic increase of T_N in Se substituted $NiPS_3$ should be ascribed to the enhanced superexchange interactions. Substituting the nonmagnetic ligand atoms is known to effectively tune superexchange in various materials [54,81–84]. In general, replacing a smaller ligand with a larger one usually leads to enhanced superexchange interaction because of the stronger orbital overlap due to greater atom orbitals [54,81]. This can be seen in our DFT calculation, which demonstrates enhanced FM for J_1 (stronger superexchange relevant for J_1 as reported previously in [78]) and J_3 for $NiPSe_3$ in comparison to $NiPS_3$ (Table I). The result of the calculation depicts the FM and AFM nature of J_1 and J_3, respectively, in the Ni system, which is consistent with the reported magnetic structure of $NiPS_3$ [25] shown in Fig. 3(d). The J_1 of both Mn and Ni systems become more ferromagnetic, but this has a different effect on the two systems due to the different magnetic order as we can see from Eqs. (2) and (3). Although both FM J_1 and AFM J_3 are enhanced upon Se substitution, the larger magnitude of J_3 (almost 4 times) than J_1 explains the stronger AFM interaction in $NiPSe_3$ than $NiPS_3$ proposed in an earlier study [67]. This also agrees well with the systematic increase of T_N with Se substitution in $NiPS_{3-x}Se_x$. Similar T_N enhancement by substituting with larger ligand atoms has also been observed in many other compounds whose magnetic interactions are mainly mediated by superexchange couplings, such as $CrCl_{3-x}Br_x$ [54] and $CuCr_{1.5}Sb_{0.5}S_{4-x}Se_x$ [82].

Though the elongation of the Ni bonds may not strongly affect exchange interactions in $NiPS_{3-x}Se_x$ as mentioned above, it may still mediate the in-plane magnetic interactions. The magnetic structure of $NiPS_3$ has a propagation vector $\mathbf{k} = [010]$ [25], where the Ni moments lie mostly within the basal plane and form a bi-collinear AFM order consisting of ferromagnetic (FM) chains along the a-axis within the Ni layer as shown in Fig. 3(d) [25,72,73]. Therefore, the expansion of the in-plane lattice would weaken the intra-chain FM couplings, which may favor the overall AFM interactions of the sample.

Though the different Se substitution-dependent ordering temperatures in $MnPS_{3-x}Se_x$ and $NiPS_{3-x}Se_x$ can be understood in terms of the mediation of magnetic exchange interactions, the very different effectiveness of tuning T_N by substitution is remaining. As shown in Figs. 2(c) and 3(c), T_N slightly decreases only by 6% from 78.5 K for $MnPS_3$ to 74 K in $MnPSe_3$, but increases remarkably in $NiPS_{3-x}Se_x$, from 155 K for $NiPS_3$ to 212 K in $NiPSe_3$. Such stronger composition dependence in $NiPS_{3-x}Se_x$ in contrast to $MnPS_{3-x}Se_x$ can be attributed to the larger magnitudes of exchange couplings J_i for Ni structures in comparison to their Mn counterparts (Table I). Moreover, as suggested by the previous neutron scattering experiment [60], $MnPSe_3$ shows stronger interlayer exchange interaction J_c than $MnPS_3$ which may stabilize the magnetic order, so the enhanced J_c with Se substitution may also offset the decrease of T_N driven by reduced intralayer exchange interaction, leading to the observed weak composition dependence in $MnPS_{3-x}Se_x$.

It is worthwhile to compare the distinct effects between chalcogen and metal substitutions in MPX_3 compounds. For polymetallic MPX_3 compounds in which the magnetic M is substituted by other magnetic or nonmagnetic metal elements, a remarkable reduction in T_N has been observed [34,37,39,46,50], which has been ascribed to the suppression of magnetic interactions by random distributions of mixed metal ions, as well as the magnetic frustrations when substituting with magnetic metal elements. Indeed, recent DFT calculation has revealed frustrations among Ni and Mn atoms in $Ni_{0.75}Mn_{0.25}PS_3$ resulting from the competing Néel and zig-zag AFM configurations [78]. The light suppression in T_N in chalcogen-substituted MPX_3 may imply weaker frustrations compared to the case of metal ion substitutions. This is also consistent with the crystal structures of MPX_3 compounds in which the chalcogen atoms are located away from the magnetic layers [Fig. 1(a)]. Therefore, substituting chalcogen layers mainly modifies the environment above and below the magnetic layers, rather than inducing strong magnetic

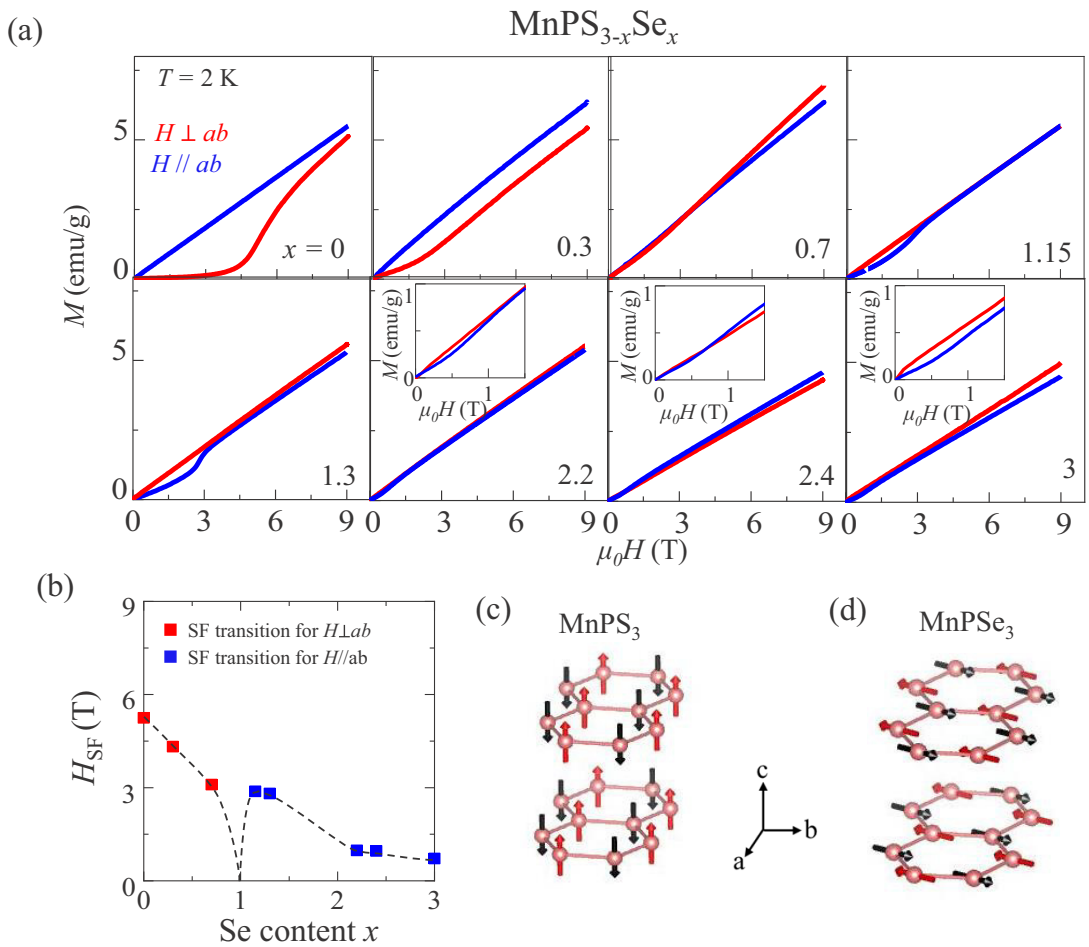

FIG. 4. (a) Field dependence of magnetization of $MnPS_{3-x}Se_x$ samples ($0 \leqslant x \leqslant 3$) at $T = 2$ K for out-of-plane ($H \perp ab$, red) and in-plane ($H \| ab$, blue) fields. Inset: Low-field magnetizations (b) Doping dependence of Spin-flop field (H_{SF}) of $MnPS_{3-x}Se_x$. (c) Magnetic structure of pristine $MnPS_3$. (d) Magnetic structure of pristine $MnPSe_3$.

impurities and magnetic dilutions for magnetic [37,39,46] and nonmagnetic [34,43] metal-ion substitutions, respectively. Hence the chalcogen substitutions could be a better approach to modify magnetism without strongly destabilizing the magnetic orderings in MPX_3.

Metal-ion substitutions in $NiPS_3$ and $MnPS_3$ have also been found to be effective in tuning magnetic anisotropies [37,39,50,52]. For example, varying the Ni:Mn ratio in $Ni_{1-x}Mn_xPS_3$ can re-orientate the magnetic easy axes from nearly within the *ab* plane to along the *c* axis [37,39]. In $NiPS_3$, Fe substitution can trigger a crossover from *XY* to Ising anisotropy [51,53]. Moreover, the magnetic anisotropy in $MnPS_3$ can be reduced with magnetic dilution by substituting nonmagnetic Zn [34,43]. In this work, we further studied the evolution of magnetic anisotropy with chalcogen substitutions. Figure 4(a) presents the isothermal field-dependent magnetization $M(H)$ at 2K for $MnPS_{3-x}Se_x$ ($0 \leqslant x \leqslant 3$) measured under out-of-plane ($H \perp ab$) and in-plane ($H//ab$) magnetic fields. The evolution of magnetic anisotropy can be extracted from the low field (i.e., below the critical field of SF transition) magnetization. The low field magnetic susceptibility is smaller with $H \perp ab$ in Se-less samples. Increasing Se content x gradually reduces anisotropy, and eventually leads the low field out-of-plane magnetization to surpass the in-plane one for $x > 0.7$. Such observation is expected since the two end compounds $MnPS_3$ and $MnPSe_3$ have different easy axis [36,43,50,70,71,85]. As shown in Figs. 4(c) and 4(d), the Mn moments in $MnPS_3$ are aligned along the out-of-plane direction [36,43], whereas they mostly lie within the basal plane with an AFM propagation vector of $\mathbf{k} = [000]$ for $MnPSe_3$ [50,70,71,85]. However, the exact in-plane directions of the moments are unclear or arbitrary based on the neutron scattering experiments on powder samples [50,70,85]. In Fig. 4(d) we depict a magnetic structure based on a recent neutron scattering study [70]. The rotation of the easy axis with Se substitution is also supported by the temperature dependent susceptibility below T_N [Fig. 2(a)], in which $\chi_\perp$ is smaller than $\chi_{//}$ for samples with x up to 0.7 but larger for samples with more Se.

The moment orientations in MPX_3 compounds are resulting from the competition between the dipolar and single-ion anisotropy, which favor an out-of-plane and an in-plane moment orientation, respectively. The single-ion anisotropy arises from the combined effects of the trigonal distortion of MX_6 octahedra and SOC [24,37]. In $MnPS_3$, the trigonal distortion and spin-orbit splitting are negligible, so its magnetism is mainly governed by the dipolar anisotropy which results in an out-of-plane moment orientation [24]. Substituting S

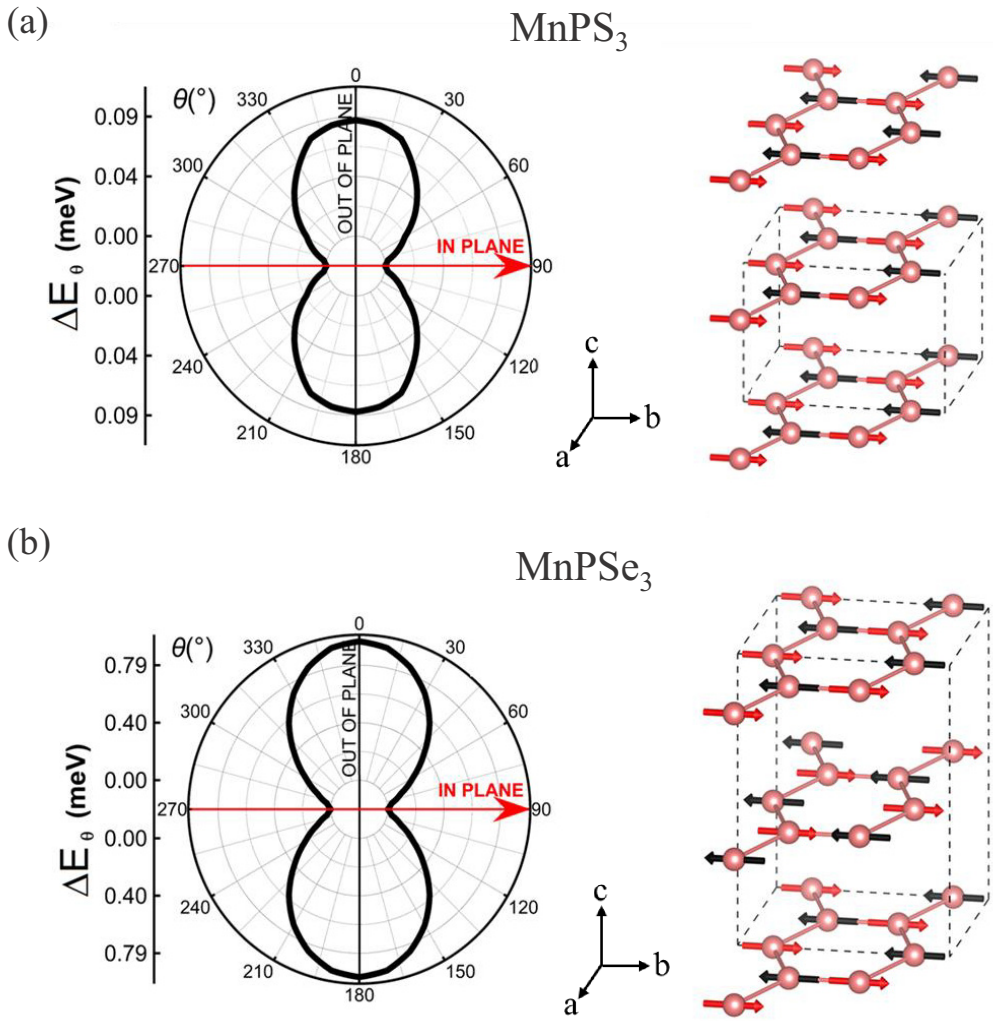

FIG. 5. (a) Left: Energy difference between the particular direction of the spins and the magnetic ground state for $MnPS_3$ system including the SOC and neglecting the magnetic dipolar interactions within the DFT studies. The latter is crucial for the proper arrangement of the spins for this system. The θ angle indicates the rotation angle from out-of-plane to in-plane position. Right: Schematic arrangement of the Mn spins in $MnPS_3$ structure. The theoretical studies predict the easy plane of magnetization in contradiction to the experimental results. (b) Left: Energy difference between the particular direction of the spins and the magnetic ground state for $MnPSe_3$ system. Right: Schematic arrangements of the Mn spins. Note, that the magnetic ordering within the layer exhibits AFM-Néel type of order, whereas the adjacent layers have antiferromagnetically aligned spins (reversed AFM-N). The easy plane of magnetization is predicted for this system.

with Se does not significantly modify trigonal distortion [70], but it causes increased ligand SOC contribution which may enhance single-ion anisotropy [71], leading to the observed moment rotation and the switching of magnetic anisotropy when $x > 0.7$. This is supported by our DFT calculation, which shows the enhancement of single-ion anisotropy (A) in $MnPSe_3$ by almost one order of magnitude as compared to $MnPS_3$ (Table I). Although the SOC that is responsible for magnetocrystalline anisotropy is accounted in our calculations, the magnetic dipolar interactions are not included in our results. Note that the very recent study has reported a developed exchange-correlation functional [86] that accounts for the magnetic dipole-dipole interactions. Considering the $MnPS_3$ system, the inclusion of the SOC causes the spins to lie within the basal plane [Fig. 5(a)]. This result is obviously in contradiction to the experimental result [Fig. 4(c)], due to the lack of the inclusion of the magnetic dipolar anisotropy in our calculations, which might align the spins to the out-of-plane direction. In addition to enhanced A, it is also plausible that long-range magnetic dipolar interactions are weakened in $MnPSe_3$ than $MnPS_3$, due to the longer lattice parameters for the Se than S compounds. Thus, the dominant A in Se-rich compounds can be ascribed to the switching of anisotropy from the out-of-plane to the in-plane direction. Furthermore, unlike $MnPS_3$ whose interlayer magnetic exchange interaction J_c is negligible, a recent neutron scattering experiment has revealed considerable J_c when S is replaced by Se [70], which is not accounted for in our theoretical results, and will be studied elsewhere. More theoretical efforts are needed to clarify the possible coupling between J_c enhancement and moment rotation.

Tuning moment orientations in MPX_3 modifies the SF transition [37,43,87]. $MnPS_3$ displays a SF transition when the magnetic field is applied along the out-of-plane direction,

which is characterized by a drastic magnetization upturn at the SF transition field (H_{SF}) [Fig. 4(a)] [5,33–37,39]. Substituting Mn with Ni is found to strongly suppress the SF transition [37,39]. H_{SF} is suppressed by half with only 5% Ni substitution, and disappears for 10% substitution, which is likely due to the reorientation of the magnetic moments when single ion anisotropy is modulated by enhanced lattice trigonal distortion upon substitution [37]. Moreover, though not as efficient as magnetic Ni substitution, the nonmagnetic Zn substitution also reduces H_{SF}, which has been ascribed to the weakening of magnetic anisotropy with magnetic dilution [43]. In this work, modification of the SF transition with Se substitution has also been observed. As shown in Fig. 4(a), at $T = 2$ K and for $H \perp ab$, the SF transition is gradually suppressed, as manifested by the less-obvious magnetization upturn and reduced H_{SF}. When Se content x is increased beyond 0.7, the observation is inverted. Magnetization displays linear field dependence when $H \perp ab$ but an upturn starts to appear under $H//ab$. Such spin flop transition occurs around ~2.9 T in the $x = 1.15$ sample, which remains strong for Se content up to $x = 1.3$ and is gradually suppressed with further increasing the Se content. For the end compound $MnPSe_3$ ($x = 3$), a small upturn around $\mu_0 H = 0.7$ T can be seen in the in-plane magnetization [Fig. 4(a), inset].

In Fig. 4(b) we summarize the variation of H_{SF} with Se content for both out-of-plane and in-plane field, from which the two types of SF transitions under $H \perp ab$ and $H//ab$ can be clearly seen. Generally, a SF transition in an AFM compound is characterized by the moment reorientation that is driven by the magnetic field component parallel to the magnetic easy axis. The change of the moment orientation can be attributed to the enhanced single-ion anisotropy upon Se substitution as discussed above, which usually favors the in-plane moment orientation. Therefore, in $MnPS_3$ whose easy axis is out-of-plane, the SF transition is characterized by Mn moment rotation toward the *ab* plane under $H \perp ab$ [36,37]. The corresponding H_{SF} is suppressed by Se substitution, because the easy axis in the substituted samples already rotates away from the out-of-plane direction.

One interesting observation is that the switching of the easy axis occurring closer to $MnPS_3$ side, i.e., between $x = 0.7$ and 1.15 [Figs. 4(a) and 4(b)], which implies the magnetism in $MnPS_3$ is softer than $MnPSe_3$. This is also consistent with our theoretical calculations. The energy difference between the in-plane and out-of-plane directions of the spins is of the order of a few hundredths of meV in $MnPS_3$ [Fig. 5(a), Left panel] and can be considered negligible ($A = -0.005$ meV, Table I), as reported in earlier works [24,72,73]. On the other hand, the energy difference in $MnPSe_3$ [Fig. 5(b), Left panel] is one order of magnitude greater than in the case of $MnPS_3$, which is reflected in the enhancement of the monocrystalline anisotropy ($A = -0.037$ meV, Table I).

Another interesting feature is that the magnetic ordering temperature does not change remarkably [Fig. 2(c)] when H_{SF} is drastically suppressed above $x = 0.7$ [Fig. 4(c)]. Similar observations have also been reported for Ni-substituted $MnPS_3$, in which the 10% Ni substitution can fully suppress the SF transition but leaves the ordering temperature essentially unchanged [37]. Such distinct composition dependences for H_{SF} and T_N have been attributed to the dominant role of the single ion anisotropy rather than the magnetic exchange in modulating SF transition [37], which may also be applicable for $MnPS_{3-x}Se_x$ studied in this work.

Similarly, the rise of SF transition for $H//ab$ is also in line with the rotation of the easy axis toward the basal plane. For the end compound $MnPSe_3$, to the best of our knowledge, the isothermal field dependent magnetization has not been reported, though this material has been known for a long time and extensively studied [50,70,71,85]. The observed weak low-field magnetization upturn is suggestive to a SF transition under in-plane magnetic field which is in line with the in-plane Mn moment orientation [Fig. 4(d)]. If the SF transition is real, the small $\mu_0 H_{SF} \approx 1$ T would be the lowest SF field reported so far in MPX_3 family [5,33–38]. Such lower H_{SF} in $MnPSe_3$ might be attributed to the distinct moment reorientation during the SF transition. For example, the moment may rotate within the basal plane so that H_{SF} is lower, unlike $MnPS_3$ whose larger H_{SF} may be related to the higher field required to overcome the anisotropy difference between its easy axis and the basal plane. A similar SF mechanism has also been proposed in another Mn system [88].

Now we turn our discussion to $NiPS_{3-x}Se_x$. As shown in Fig. 6(a), consistent with the earlier magnetization studies [37,39], a metamagnetic spin flop transition under an in-plane field of ~6 T can be seen in isothermal magnetization measurements. Such observation also agrees with the nearly in-plane orientation for Ni moments [25] due to strong single-ion anisotropy in $NiPS_3$ [72,73]. Se substitution leads the SF transition to occur at a higher in-plane field of around 8 T for $x = 0.25$. Further increasing Se content leads to essentially linear field-dependent magnetization for both $H//ab$ and $H \perp ab$ up to 9 T. The increased H_{SF} with Se substitution in $NiPS_3$ is in sharp contrast to observation in $MnPS_{3-x}Se_x$ [Fig. 4(b)]. Unlike the $MnPS_{3-x}Se_x$ system for which the magnetic structure for end compounds $MnPS_3$ [36,43] and $MnPSe_3$ [50,70,71,85] have been well understood, the lack of the established magnetic structure for $NiPSe_3$ makes it difficult to clarify how Ni moment orientation may play a role in the observed substitution dependence of H_{SF} in $NiPS_{3-x}Se_x$. Our DFT calculation has demonstrated the out-of-plane moment orientation for $NiPSe_3$ [Fig. 6(b)]. This agrees well with the possible higher H_{SF} required for Se-rich samples, in a manner similar to $MnPS_{3-x}Se_x$, where SF transition occurs at higher H_{SF} for compounds ($x = 0$–0.7) with the easy axis along an out-of-plane direction. In addition to the orientation of the easy axis, the stronger exchange interaction in Se-substituted $NiPS_3$ may be another possible factor that affects the H_{SF}. The SF field at low temperatures can be approximately expressed as $H_{SF} \approx \sqrt{2H_E H_A}$ where H_E and H_A are effective exchange and magnetic anisotropy fields, respectively [88]. Since Se substitution enhances the exchange interactions as discussed earlier, increased H_{SF} is expected. To better clarify the mechanism for the evolution of SF transition in $NiPS_{3-x}Se_x$, future neutron scattering experiments even on polycrystalline samples, magnetization measurements under high magnetic field, and theoretical efforts would be helpful.

In conclusion, we studied the magnetic properties of previously unreported Se-substituted $MnPS_3$ and $NiPS_3$. We found distinct tuning of T_N in $MnPS_{3-x}Se_x$ and $NiPS_{3-x}Se_x$, likely attributed to different exchange interactions in pristine

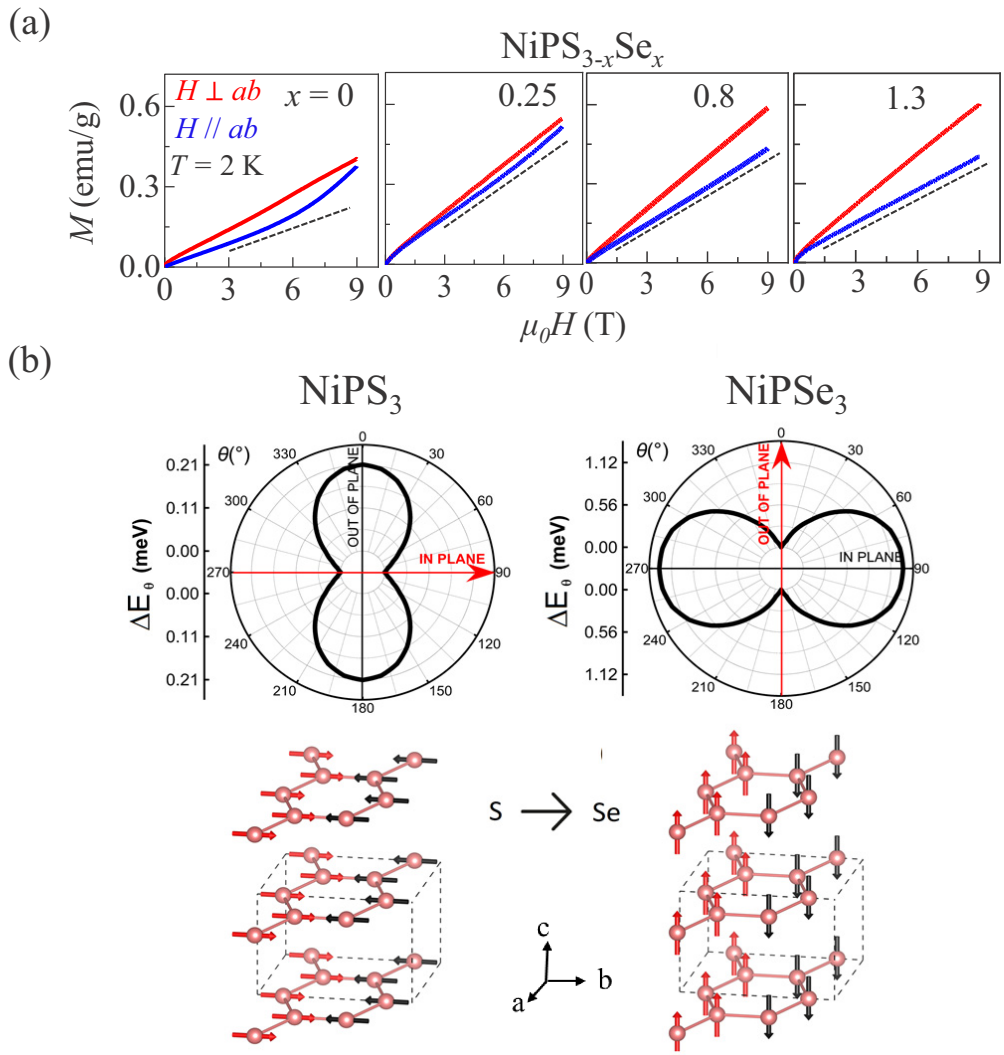

FIG. 6. (a) Field dependence of magnetization of $NiPS_{3-x}Se_x$ samples ($0 \leqslant x \leqslant 1.3$) at $T = 2$ K for out-of-plane ($H \perp ab$, red) and in-plane ($H||ab$, blue) fields. The dashed lines are a guide to the eye. (b) Upper panels: Energy difference between the particular directions of the spins and the magnetic ground state for $NiPS_3$ and $NiPSe_3$ using DFT calculations. The spins of the Ni atoms are collinearly aligned. The θ angle indicates the rotation angle from out-of-plane to in-plane position. The changes in rotation angle within the layer are negligible (negligible difference between the spins oriented in a and b directions). Lower panels: Schematic pictures of magnetic spins for $NiPS_3$ and $NiPSe_3$. Note that, the $NiPS_3$ exhibits an easy plane (XY) of magnetization, whereas the $NiPSe_3$ has an easy axis oriented perpendicular to the layer.

$MnPS_3$ and $NiPS_3$. In addition, the magnetic anisotropy is also efficiently modulated with S-Se substitutions. Our findings provide a suitable platform for a deeper understanding of low-dimensional magnetism and potential spintronics applications.

ACKNOWLEDGMENTS

Experimental work at the University of Arkansas (crystal growth and measurements) is supported by the U.S. Department of Energy, Office of Science, Basic Energy Sciences program under Grant No. DE-SC0022006. We acknowledge the support from the Open Access Publishing Fund administered through the University of Arkansas Libraries for open access publication. C.A. is supported by the Foundation for Polish Science through the International Research Agendas program cofinanced by the European Union within the Smart Growth Operational Programme. M.B. acknowledges support by the University of Warsaw within the project "Excellence Initiative-Research University" programme. Access to computing facilities of PL-Grid Polish Infrastructure for Supporting Computational Science in the European Research Space and of the Interdisciplinary Center of Modeling (ICM), University of Warsaw are gratefully acknowledged. Financial support from the University of Warsaw under the "Excellence Initiative-Research University" project is acknowledged by M.B. We made use of computing facilities of TU Dresden ZIH within the project "TransPheMat".

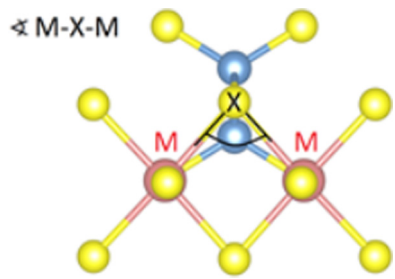

FIG. 7. (a) Schematic picture of the bond angle between the metal and chalcogen atoms (∢M-X-M),crucial for the indirect superexchange mechanism. The blue balls indicate the P atoms.

APPENDIX: THEORETICAL EXCHANGE COUPLINGS

The exchange parameters derived from the Heisenberg Hamiltonian (1):

$$E^x_{FM} = E_0 - \frac{1}{2}(3J_1S^2 + 6J_2S^2 + 3J_3S^2),$$

$$E^x_{\text{Neel}} = E_0 - \frac{1}{2}(-3J_1S^2 + 6J_2S^2 - 3J_3S^2),$$

$$E^x_{\text{zigzag}} = E_0 - \frac{1}{2}(J_1S^2 - 2J_2S^2 - 3J_3S^2),$$

$$E^x_{\text{stripy}} = E_0 - \frac{1}{2}(-J_1S^2 - 2J_2S^2 + 3J_3S^2),$$

$$E^z_{FM} - E^x_{FM} = \frac{-1}{2}(3\lambda_1S^2 + 6\lambda_2S^2 + 3\lambda_3S^2) - AS^2,$$

$$E^z_{\text{Neel}} - E^x_{\text{Neel}} = \frac{-1}{2}(-3\lambda_1S^2 + 6\lambda_2S^2 - 3\lambda_3S^2) - AS^2,$$

$$E^z_{\text{zigzag}} - E^x_{\text{zigzag}} = \frac{-1}{2}(\lambda_1S^2 - 2\lambda_2S^2 - 3\lambda_3S^2) - AS^2,$$

$$E^z_{\text{stripy}} - E^x_{\text{stripy}} = \frac{-1}{2}(-\lambda_1S^2 - 2\lambda_2S^2 + 3\lambda_3S^2) - AS^2,$$

$$J_1 = \frac{1}{4S^2}\left(-E^x_{\text{zigzag}} + E^x_{\text{stripy}} - E^x_{FM} + E^x_{\text{Neel}}\right),$$

$$J_2 = \frac{1}{8S^2}\left(E^x_{\text{zigzag}} + E^x_{\text{stripy}} - E^x_{FM} - E^x_{\text{Neel}}\right),$$

$$J_3 = \frac{1}{12S^2}\left(3E^x_{\text{zigzag}} - 3E^x_{\text{stripy}} - E^x_{FM} + E^x_{\text{Neel}}\right),$$

$$\lambda_1 = \frac{1}{4S^2}(-\Delta E_{\text{zigzag}} + \Delta E_{stipy} - \Delta E_{FM} + \Delta E_{\text{Neel}}),$$

$$\lambda_2 = \frac{1}{8S^2}(\Delta E_{\text{zigzag}} + \Delta E_{\text{stripy}} - \Delta E_{FM} - \Delta E_{\text{Neel}}),$$

$$\lambda_3 = \frac{1}{12S^2}(3\Delta E_{\text{zigzag}} - 3\Delta E_{\text{stripy}} - \Delta E_{FM} + \Delta E_{\text{Neel}}),$$

$$A = \frac{1}{8S^2}(3\Delta E_{\text{zigzag}} + 3\Delta E_{\text{stripy}} + \Delta E_{FM} + \Delta E_{\text{Neel}}),$$

$$\Delta E = E^z - E^x.$$

Note, that the equations for λ_3 and J_3 are different than obtained in Ref. [9].

[1] B. Huang *et al.*, Layer-Dependent ferromagnetism in a van der Waals crystal down to the monolayer limit, Nature (London) **546**, 270 (2017).

[2] C. Gong *et al.*, Discovery of intrinsic ferromagnetism in two-dimensional van der Waals crystals, Nature (London) **546**, 265 (2017).

[3] Z. Fei *et al.*, Two-Dimensional itinerant ferromagnetism in atomically thin Fe_3GeTe_2, Nat. Mater. **17**, 778 (2018).

[4] X. Cai *et al.*, Atomically thin $CrCl_3$: an in-plane layered antiferromagnetic insulator, Nano Lett. **19**, 3993 (2019).

[5] G. Long, H. Henck, M. Gibertini, D. Dumcenco, Z. Wang, T. Taniguchi, K. Watanabe, E. Giannini, and A. F. Morpurgo, Persistence of magnetism in atomically thin $MnPS_3$ crystals Nano Lett. **20**, 2452 (2020).

[6] L. Kang *et al.*, Phase-Controllable growth of ultrathin 2D magnetic FeTe crystals, Nat. Commun. **11**, 3729 (2020).

[7] S. Albarakati *et al.*, Antisymmetric magnetoresistance in van der Waals Fe_3GeTe_2/Graphite/Fe_3GeTe_2 trilayer heterostructures, Sci. Adv. **5**, eaaw0409 (2019).

[8] S. Jiang, L. Li, Z. Wang, K. F. Mak, and J. Shan, Controlling magnetism in 2D CrI_3 by electrostatic doping, Nat. Nanotechnol. **13**, 549 (2018).

[9] Z. Wang *et al.*, Electric-Field control of magnetism in a few-layered van der Waals ferromagnetic semiconductor, Nat. Nanotechnol. **13**, 554 (2018).

[10] B. Huang *et al.*, Electrical control of 2D magnetism in bilayer CrI_3, Nat. Nanotechnol. **13**, 544 (2018).

[11] Y. Deng *et al.*, Gate-Tunable room-temperature ferromagnetism in two-dimensional Fe_3GeTe_2, Nature (London) **563**, 94 (2018).

[12] T. Song *et al.*, Giant tunneling magnetoresistance in spin-filter van der Waals heterostructures, Science **360**, 1214 (2018).

[13] Y. Wu *et al.*, Néel-type Skyrmion in WTe_2/Fe_3GeTe_2 van der Waals heterostructure, Nat. Commun. **11**, 3860 (2020).

[14] D. R. Klein *et al.*, Probing magnetism in 2D van der Waals crystalline insulators via electron tunneling, Science **360**, 1218 (2018).

[15] J. Shang, X. Tang, X. Tan, A. Du, T. Liao, S. C. Smith, Y. Gu, C. Li, and L. Kou, Stacking-dependent interlayer magnetic coupling in 2D CrI_3/$CrGeTe_3$ nanostructures for Spintronics, ACS Appl. Nano Mater. **3**, 1282 (2020).

[16] D. Zhong *et al.*, Van der Waals engineering of ferromagnetic semiconductor heterostructures for spin and valleytronics, Sci. Adv. **3**, e1603113 (2017).

[17] Z. Wang, I. Gutiérrez-Lezama, N. Ubrig, M. Kroner, M. Gibertini, T. Taniguchi, K. Watanabe, A. Imamoğlu, E. Giannini, and A. F. Morpurgo, Very large tunneling magnetoresistance in layered magnetic semiconductor CrI_3, Nat. Commun. **9**, 2516 (2018).

[18] T. Song *et al.*, Voltage control of a van der Waals spin-filter magnetic tunnel junction, Nano Lett. **19**, 915 (2019).

[19] Y. Wang *et al.*, Modulation doping via a two-dimensional atomic crystalline acceptor, Nano Lett. **20**, 8446 (2020).

[20] G. Ouvrard, R. Brec, and J. Rouxel, Structural determination

of some MPS_3 layered phases (M = Mn, Fe, Co, Ni and Cd), Mater. Res. Bull. **20**, 1181 (1985).

[21] W. Klingen, G. Eulenberger, and H. Hahn, About the crystal structures of $Fe_2P_2Se_6$ and $Fe_2P_2S_6$, Z. Anorg. Alleg. Chem. **401**, 97 (1973).

[22] K. Du, X. Wang, Y. Liu, P. Hu, M. I. B. Utama, C. K. Gan, Q. Xiong, and C. Kloc, Weak van der Waals Stacking, wide-range band Gap, and raman study on ultrathin layers of metal phosphorus trichalcogenides, ACS Nano **10**, 1738 (2016).

[23] F. Wang *et al.*, New frontiers on van der Waals layered metal phosphorous trichalcogenides, Adv. Funct. Mater. **28**, 1802151 (2018).

[24] P. A. Joy and S. Vasudevan, Magnetism in the layered transition-metal thiophosphates MPS_3 (M = Mn, Fe, and Ni), Phys. Rev. B **46**, 5425 (1992).

[25] A. R. Wildes, V. Simonet, E. Ressouche, G. J. Mcintyre, M. Avdeev, E. Suard, S. A. Kimber, D. Lançon, G. Pepe, and B. Moubaraki, Magnetic structure of the quasi-two-dimensional antiferromagnet $NiPS_3$, Phys. Rev. B **92**, 224408 (2015).

[26] K. C. Rule, G. J. McIntyre, S. J. Kennedy, and T. J. Hicks, Single-Crystal and powder neutron diffraction experiments on $FePS_3$: Search for the magnetic structure, Phys. Rev. B **76**, 134402 (2007).

[27] A. R. Wildes, H. M. Rønnow, B. Roessli, M. J. Harris, and K. W. Godfrey, Static and dynamic critical properties of the quasi-two-dimensional antiferromagnet $MnPS_3$, Phys. Rev. B **74**, 094422 (2006).

[28] D. Lançon, H. C. Walker, E. Ressouche, B. Ouladdiaf, K. C. Rule, G. J. McIntyre, T. J. Hicks, H. M. Rønnow, and A. R. Wildes, Magnetic structure and magnon dynamics of the quasi-two-dimensional antiferromagnet $FePS_3$, Phys. Rev. B **94**, 214407 (2016).

[29] A. R. Wildes, B. Roessli, B. Lebech, and K. W. Godfrey, Spin waves and the critical behaviour of the magnetization in $MnPS_3$, J. Phys.: Condens. Matter **10**, 6417 (1998).

[30] A. R. Wildes, V. Simonet, E. Ressouche, R. Ballou, and G. J. McIntyre, The magnetic properties and structure of the quasi-two-dimensional antiferromagnet $CoPS_3$, J. Phys.: Condens. Matter **29**, 455801 (2017).

[31] T. Sekine, M. Jouanne, C. Julien, and M. Balkanski, Light-Scattering study of dynamical behavior of antiferromagnetic spins in the layered magnetic semiconductor $FePS_3$, Phys. Rev. B **42**, 8382 (1990).

[32] Y. Takano, N. Arai, A. Arai, Y. Takahashi, K. Takase, and K. Sekizawa, Magnetic properties and specific heat of MPS_3 (M = Mn, Fe, Zn), J. Magn. Magn. Mater. **272–276**, E593 (2004).

[33] G. Long *et al.*, Isolation and characterization of few-layer manganese thiophosphite, ACS Nano **11**, 11330 (2017).

[34] D. J. Goossens and T. J. Hicks, The magnetic phase diagram of $Mn_xZn_{1-x}PS_3$, J. Phys.: Condens. Matter **10**, 7643 (1998).

[35] K. Okuda, K. Kurosawa, S. Saito, M. Honda, Z. Yu, and M. Date, Magnetic properties of layered compound $MnPS_3$, J. Phys. Soc. Jpn. **55**, 4456 (1986).

[36] D. J. Goossens, A. R. Wildes, C. Ritter, and T. J. Hicks, Ordering and the nature of the spin flop phase transition in $MnPS_3$, J. Phys.: Condens. Matter **12**, 1845 (2000).

[37] R. Basnet, A. Wegner, K. Pandey, S. Storment, and J. Hu, Highly sensitive spin-flop transition in antiferromagnetic van der Waals material MPS_3(M = Ni and Mn), Phys. Rev. Materials **5**, 064413 (2021).

[38] A. R. Wildes, D. Lançon, M. K. Chan, F. Weickert, N. Harrison, V. Simonet, M. E. Zhitomirsky, M. V. Gvozdikova, T. Ziman, and H. M. Rønnow, High field magnetization of $FePS_3$, Phys. Rev. B **101**, 024415 (2020).

[39] Y. Shemerliuk, Y. Zhou, Z. Yang, G. Cao, A. U. B. Wolter, B. Büchner, and S. Aswartham, Tuning magnetic and transport properties in Quasi-2D $(Mn_{1-x}Ni_x)_2P_2S_6$ single crystals, Electron. Mater. **2**, 284 (2021).

[40] D. Afanasiev *et al.*, Controlling the anisotropy of a van der Waals antiferromagnet with light, Sci. Adv. **7**, eabf3096 (2021).

[41] N. Chandrasekharan and S. Vasudevan, Dilution of a layered antiferromagnet: Magnetism in $Mn_xZn_{1-x}PS_3$, Phys. Rev. B **54**, 14903 (1996).

[42] D. J. Goossens, A. J. Studer, S. J. Kennedy, and T. J. Hicks, The impact of magnetic dilution on magnetic order in $MnPS_3$, J. Phys.: Condens. Matter **12**, 4233 (2000).

[43] A. M. Mulders, J. C. P. Klaasse, D. J. Goossens, J. Chadwick, and T. J. Hicks, High-Field magnetization in the diluted quasi-two-dimensional heisenberg antiferromagnet $Mn_{1-x}Zn_xPS_3$, J. Phys.: Condens. Matter **14**, 8697 (2002).

[44] Y. Takano, A. Arai, Y. Takahashi, K. Takase, and K. Sekizawa, Magnetic properties and specific heat of new spin glass $Mn_{0.5}Fe_{0.5}PS_3$, J. Appl. Phys. **93**, 8197 (2003).

[45] J. N. Graham, M. J. Coak, S. Son, E. Suard, J.-G. Park, L. Clark, and A. R. Wildes, Local nuclear and magnetic order in the two-dimensional spin glass $Mn_{0.5}Fe_{0.5}PS_3$, Phys. Rev. Materials **4**, 084401 (2020).

[46] T. Masubuchi, H. Hoya, T. Watanabe, Y. Takahashi, S. Ban, N. Ohkubo, K. Takase, and Y. Takano, Phase diagram, Magnetic properties and Specific Heat of $Mn_{1-x}Fe_xPS_3$, J. Alloys Compd. **460**, 668 (2008).

[47] V. Manrıquez, P. Barahona, and O. Peña, Physical properties of the cation-mixed $M'MPS_3$ phases, Mater. Res. Bull. **35**, 1889 (2000).

[48] D. J. Goossens, S. Brazier-Hollins, D. R. James, W. D. Hutchison, and J. R. Hester, Magnetic structure and glassiness in $Fe_{0.5}Ni_{0.5}PS_3$, J. Magn. Magn. Mater. **334**, 82 (2013).

[49] Y. He, Y.-D. Dai, H. Huang, J. Lin, and Y. Hsia, The ordering distribution of the metal ions in the layered cation-mixed phosphorus trisulfides $Mn_xFe_{1-x}PS_3$, J. Alloys Compd. **359**, 41 (2003).

[50] A. Bhutani, J. L. Zuo, R. D. McAuliffe, C. R. dela Cruz, and D. P. Shoemaker, Strong anisotropy in the mixed antiferromagnetic system $Mn_{1-x}Fe_xPSe_3$, Phys. Rev. Materials **4**, 034411 (2020).

[51] S. Selter, Y. Shemerliuk, M.-I. Sturza, A. U. B. Wolter, B. Büchner, and S. Aswartham, Crystal growth and anisotropic magnetic properties of quasi-two-dimensional $(Fe_{1-x}Ni_x)_2P_2S_6$, Phys. Rev. Materials **5**, 073401 (2021).

[52] F. Wang *et al.*, Defect-mediated ferromagnetism in correlated two-dimensional transition metal phosphorus trisulfides, Sci. Adv. **7**, eabj4086 (2021).

[53] S. Lee, J. Park, Y. Choi, K. Raju, W.-T. Chen, R. Sankar, and K.-Y. Choi, Chemical tuning of magnetic anisotropy and correlations in $Ni_{1-x}Fe_xPS_3$, Phys. Rev. B **104**, 174412 (2021).

[54] M. Abramchuk, S. Jaszewski, K. R. Metz, G. B. Osterhoudt, Y. Wang, K. S. Burch, and F. Tafti, Controlling magnetic and

optical properties of the van der Waals crystal $CrCl_{3-x}Br_x$ via mixed halide chemistry, Adv. Mater. **30**, 1801325 (2018).

[55] T. A. Tartaglia *et al.*, Accessing new magnetic regimes by tuning the ligand spin-orbit coupling in van der Waals magnets, Sci. Adv. **6**, eabb9379 (2020).

[56] X. Yan, X. Chen, and J. Qin, Synthesis and magnetic properties of layered $MnPS_xSe_{3-x}$ ($0 < x < 3$) and corresponding intercalation compounds of 2,2′-bipyridine, Mater. Res. Bull. **46**, 235 (2011).

[57] G. Kliche, Infrared spectra of the hexachalcogenohypodiphosphate mixed crystals $Co_{2-x}Ni_xP_2S_6$ and $Ni_2P_2S_{6-x}Se_x$, Z. Naturforsch. A **38**, 1133 (1983).

[58] B. Zapeka, M. Kostyrko, I. Martynyuk-Lototska, and R. Vlokh, Critical behaviour of $Sn_2P_2S_6$ and $Sn_2P_2(Se_{0.28}S_{0.72})_6$ crystals under high hydrostatic pressures, Philos. Mag. **95**, 382 (2015).

[59] B. Hillman, L. Noren, and D. J. Goossens, Structural properties of compounds in the $MPS_{3-x}Se_x$ family, in *Proceedings of the 35th Annual Australia/New Zealand Condensed Matter and Materials Meeting*, 50 (Australian Institute of Physics, Wagga, 2011).

[60] S. L. Dudarev, G. A. Botton, S. Y. Savrasov, C. J. Humphreys, and A. P. Sutton, Electron-energy-loss spectra and the structural stability of nickel oxide: An LSDA+U study, Phys. Rev. B **57**, 1505 (1998).

[61] G. Kresse and J. Hafner, *Ab initio* molecular dynamics for liquid metals, Phys. Rev. B **47**, 558 (1993).

[62] G. Kresse and J. Furthmüller, Efficiency of *ab initio* total energy calculations for metals and semiconductors using a plane-wave basis set, Comput. Mater. Sci. **6**, 15 (1996).

[63] M. Birowska, K. Milowska, and J. Majewski, Van der Waals density functionals for graphene layers and graphite, Acta Phys. Pol. A **120**, 845 (2011).

[64] K. Milowska, M. Birowska, and J. A. Majewski, Mechanical, Electrical, and magnetic properties of functionalized carbon nanotubes, AIP Conf. Proc. **1399**, 827 (2011).

[65] M. Birowska, M. E. Marchwiany, C. Draxl, and J. A. Majewski, Assessment of approaches for dispersive forces employing semihydrogenated graphene as a case Study, Computat. Mater. Sci. **186**, 109940 (2021).

[66] S. Grimme, J. Antony, S. Ehrlich, and H. Krieg, a consistent and accurate *ab initio* parametrization of density functional dispersion correction (DFT-D) for the 94 elements H-Pu, J. Chem. Phys. **132**, 154104 (2010).

[67] G. Le Flem, R. Brec, G. Ouvard, A. Louisy, and P. Segransan, Magnetic interactions in the layer compounds MPX_3 (M = Mn, Fe, Ni; X = S, Se), J. Phys. Chem. Solids **43**, 455 (1982).

[68] A. P. Dioguardi, S. Selter, U. Peeck, S. Aswartham, M.-I. Sturza, R. Murugesan, M. S. Eldeeb, L. Hozoi, B. Büchner, and H.-J. Grafe, Quasi-two-dimensional magnetic correlations in $Ni_2P_2S_6$ probed by ^{31}P NMR, Phys. Rev. B **102**, 064429 (2020).

[69] N. Chandrasekharan and S. Vasudevan, Magnetism and exchange in the layered antiferromagnet $NiPS_3$, J. Phys.: Condens. Matter **6**, 4569 (1994).

[70] S. Calder, A. V. Haglund, A. I. Kolesnikov, and D. Mandrus, Magnetic exchange interactions in the van der Waals layered antiferromagnet $MnPSe_3$, Phys. Rev. B **103**, 024414 (2021).

[71] P. Jeevanandam and S. Vasudevan, Magnetism in $MnPSe_3$: a layered $3d^5$ antiferromagnet with unusually large XY anisotropy, J. Phys.: Condens. Matter **11**, 3563 (1999).

[72] D. Lançon, R. A. Ewings, T. Guidi, F. Formisano, and A. R. Wildes, Magnetic exchange parameters and anisotropy of the quasi-two-dimensional antiferromagnet $NiPS_3$, Phys. Rev. B **98**, 134414 (2018).

[73] C. Kim, J. Jeong, P. Park, T. Masuda, S. Asai, S. Itoh, H.-S. Kim, A. Wildes, and J.-G. Park, Spin waves in the two-dimensional honeycomb lattice XXZ-type van der Waals antiferromagnet $CoPS_3$, Phys. Rev. B **102**, 184429 (2020).

[74] Y. Gu, Q. Zhang, C. Le, Y. Li, T. Xiang, and J. Hu, Ni-Based transition metal trichalcogenide Monolayer: A strongly correlated quadruple-layer graphene, Phys. Rev. B **100**, 165405 (2019).

[75] K. Kurosawa, S. Saito, and Y. Yamaguchi, Neutron diffraction study on $MnPS_3$ and $FePS_3$, J. Phys. Soc. Jpn. **52**, 3919 (1983).

[76] M. Birowska, P. E. Faria Junior, J. Fabian, and J. Kunstmann, Large exciton binding energies in $MnPS_3$ as a case study of a van der Waals layered magnet, Phys. Rev. B **103**, L121108 (2021).

[77] T. Olsen, Magnetic anisotropy and exchange interactions of two-dimensional $FePS_3$, $NiPS_3$ and $MnPS_3$ from first principles calculations, J. Phys. D **54**, 314001 (2021).

[78] C. Autieri, G. Cuono, C. Noce, M. Rybak, K. M. Kotur, C. E. Agrapidis, K. Wohlfeld, and M. Birowska, Limited ferromagnetic interactions in monolayers of MPS_3 (M = Mn and Ni), J. Phys. Chem. C **126**, 6791 (2022).

[79] J. B. Goodenough, Theory of the role of covalence in the perovskite-type manganites [La, M(II)]MnO_3, Phys. Rev. **100**, 564 (1955).

[80] J. Kanamori, Superexchange interaction and symmetry properties of electron orbitals, J. Phys. Chem. Solids **10**, 87 (1959).

[81] S. Kobayashi, H. Ueda, C. Michioka, and K. Yoshimura, Competition between the direct exchange interaction and superexchange interaction in layered compounds $LiCrSe_2$, $LiCrTe_2$, and $NaCrTe_2$ with a triangular lattice, Inorg. Chem. **55**, 7407 (2016).

[82] T. G. Aminov, G. G. Shabunina, and E. V. Busheva, Synthesis and magnetic properties of $CuCr_{1.5}Sb_{0.5}S_{4-x}Se_x$ solid solutions, Russ. J. Inorg. Chem. **57**, 1428 (2012).

[83] C. Pughe *et al.*, Site-selective d^{10}/d^0 substitution in an $s = 1/2$ spin ladder $Ba_2CuTe_{1-x}W_xO_6$ ($0 \leqslant x \leqslant 0.3$), Inorg. Chem. **61**, 4033 (2022).

[84] V. M. Katukuri, P. Babkevich, O. Mustonen, H. C. Walker, B. Fåk, S. Vasala, M. Karppinen, H. M. Rønnow, and O. V. Yazyev, Exchange Interactions Mediated by Nonmagnetic Cations in Double Perovskites, Phys. Rev. Lett. **124**, 077202 (2020).

[85] A. Wiedenmann, J. Rossat-Mignod, A. Louisy, R. Brec, and J. Rouxel, Neutron diffraction study of the layered compounds $MnPSe_3$ and $FePSe_3$, Solid State Commun. **40**, 1067 (1981).

[86] C. Pellegrini, T. Müller, J. K. Dewhurst, S. Sharma, A. Sanna, and E. K. U. Gross, Density functional theory of magnetic dipolar interactions, Phys. Rev. B **101**, 144401 (2020).

[87] D. J. Goossens, Dipolar anisotropy in quasi-2D honeycomb antiferromagnet $MnPS_3$, Eur. Phys. J. B **78**, 305 (2010).

[88] Y. Yu, G. Deng, Y. Cao, G. J. McIntyre, R. Li, N. Yuan, Z. Feng, J.-Y. Ge, J. Zhang, and S. Cao, Tuning the magnetic anisotropy via Mn substitution in single crystal $Co_4Nb_2O_9$, Ceram. Int. **45**, 1093 (2019).